PHYSICAL REVIEW C VOLUME 22, NUMBER 4 OCTOBER 1980

Recoil ranges of nuclei produced in the interaction of 80–164 MeV protons with Ni

J. Jastrzebski,* H. J. Karwowski,† M. Sadler,‡ and P. P. Singh
Indiana University Cyclotron Facility, Bloomington, Indiana 47405
(Received 27 February 1980)

Cross sections and effective recoil ranges of nuclei produced in the 80, 136, 153, and 164 MeV proton bombardment of ^{58}Ni and ^{62}Ni targets have been measured using the conventional thick target recoil catcher technique. The measured ranges increase monotonically with the number of nucleons removed from the target, and only for the lightest of the product nuclei are they comparable to values expected for compound nucleus formation. This trend is consistent with the picture in which the initial proton-nucleus interactions leave a few intermediate nuclei over a broad range of excitation, from which the bulk of the final nuclei are produced by evaporation. Detailed comparisons of the observations with predictions of the cascade model are presented and discussed.

[NUCLEAR REACTIONS ^{58}Ni(p,X), ^{62}Ni(p,X), E=80–164 MeV. Measured E_γ, I_γ of radioactive products; deduced $\sigma(X,E)$, recoil ranges, mass distribution, charge distribution. Enriched targets, Ge(Li) counting.]

I. INTRODUCTION

We recently[1,2] reported cross sections with which various residual nuclei were produced following 80–164 MeV proton bombardment of targets of even mass (58–64) isotopes of nickel. The production cross sections were determined using the absolute yields of characteristic γ rays belonging to each final nucleus as seen in measured in-beam γ-ray energy spectra at various energies, supplemented by cross sections for the production of radioactive species reported more fully in this paper. From the systematics of the observed cross sections we were able to decipher a few features of the partitioning of the incident energy into that carried away by outgoing fast (in contrast to evaporation) particles, and that left as nuclear excitation. For example, it was concluded that in the above incident energy range, on the average, from $\frac{1}{2}$ to $\frac{2}{3}$ of the incident energy is taken away by fast outgoing particles, leaving the remainder as nuclear excitation.

Quantitatively, the measured cross sections were compared with the predictions of cascade[3] and exciton models.[4,5] These models envision the nucleon-nucleus interaction as a sequence of nucleon-nucleon interactions, initiated by the incident nucleon, at each step of which there is a finite probability for one, both, or neither of the particles to escape from the nuclear environment without further interaction. Thus, a part of the incident energy is carried out by the escaping particles (generally referred to as pre-equilibrium emission), while the rest remains in the nucleus which dissipates it through statistical (equilibrium) emissions. Both models were able to give an adequate account of the observed cross sections.

Energy partitioning is but one characteristic of any interactional mechanism; others are momentum and angular momentum transfers. The work reported here relates to measurements of the recoil ranges of the nuclei produced with a view of getting experimental information about the momentum transfer associated with specific final nuclei. The aim was to seek clues about some aspect of the interaction from the trends and magnitudes of the observed ranges and also to test the model predictions with another variable (momentum transfer) characteristic of any interaction. There exist many studies in which measurement of recoil ranges of spallation residues with medium to high energy proton bombardment have been reported along with comparison with the predictions of the cascade model (see, e.g., Refs. 6–9). Whereas, in general, the earlier studies have concentrated on measuring recoil ranges of one or a few nuclei, we report here measurement of the recoil ranges of nuclei essentially covering the whole mass range of the nuclear products. Further, we present a comparison of the measured recoil ranges for all nuclei to the predictions of the cascade model, including the effects of evaporation. The trends in the observed ranges allow us to draw conclusions about the interaction processes.

II. EXPERIMENTAL METHOD AND RESULTS

Measurements reported here were made using 80-, 136-, 153-, and 164-MeV proton beams of about 100 nA intensity obtained at the Indiana University Cyclotron Facility. The method used to measure the integral ranges of recoiling nuclei

was a conventional one and consisted of bombarding self-supporting foils of ^{58}Ni or ^{62}Ni sandwiched between aluminum or kapton catchers. The uniformity and thickness of the target foils were measured using the energy loss of α particles from a ^{241}Am source and comparing it with the values obtained from the tables of Ref. 10. Target thicknesses were found to be uniform within 10%. Target composition and thicknesses are given in Table I. The thickness of the catchers was chosen so that the most energetic recoils would stop. Transmitted beam was collected in a three section Faraday cup and measured using a calibrated charge integrator. Irradiation times for different bombardments were between 1 and 4 h.

Gamma-ray energy spectra from the irradiated Ni targets and their associated forward and backward catchers were recorded, using a Ge(Li) detector, beginning about 10 min after the end of the bombardment and continuing over a period extending up to 3 months thereafter. Details of these measurements and attribution of the observed γ rays to a particular final nucleus were the same as described elsewhere.[11]

If R_F is the average forward (backward) recoil range in Ni, and $\theta_F(\theta_B)$ is the average forward (backward) recoiling angle of a particular final nuclei, then only those nuclei which are produced in the last (first) segment of the target, $R_f \cos\theta_F$ ($R_B \cos\theta_B$), will be able to escape into the forward (backward) catchers. Assuming nuclei are produced uniformly throughout the target, the ratio of the activity measured in the forward (backward) catchers to the total activity (of that in the target and the catcher) times the target thickness T is a measure of the projected effective forward (backward) recoil ranges[12]:

$$R = T\frac{A_F}{A_F + A_T},$$

where A_F and A_T is the activity of a given reaction product observed in the catcher and target foils, respectively. The activity measured on the backward catcher A_B was used to determine the backward to forward ratios defined as $B/F = A_B/A_F$.

From the observed total activities and the known half-lives, the production cross sections of various final nuclei were also deduced. In Tables II and III the measured production cross sections, effective forward ranges R, and B/F ratios for the radioactive products are listed for ^{58}Ni and ^{62}Ni targets. The recoil ranges as a function of the number of nucleons removed, ΔA, ($\equiv A_{\text{target}}$ minus A_{product}) are also presented in the following section in Figs. 4–7 and the B/F ratios are presented in Fig. 11.

The "true" average projected ranges can differ from the effective ranges defined above. Let x be the fraction of a given product recoiling forward, $(1-x)$ the corresponding fraction recoiling backward, N the number of nuclei produced in a unit length of target thickness, and R_F and R_B the true forward and backward projected ranges. The following relations may be written:

$$A_F = xNR_F,$$

$$A_B = (1-x)NR_B,$$

$$A_T = NT - A_F - A_B.$$

From the above it follows that

$$\frac{R}{T} = \frac{A_F}{A_F + A_T} = \frac{xR_F}{T - R_B(1-x)}.$$

If x is close to unity one can neglect the last term

TABLE I. Target composition and thicknesses.

Target	Target composition (%) ^{58}Ni	^{60}Ni	^{61}Ni	^{62}Ni	^{64}Ni	Bombarding energy (MeV)	Target thickness [a] (mg/cm^2)
^{58}Ni	99.89	0.11	<0.01	<0.01	<0.01	80	3.27
						153	4.88
						164	3.38
^{62}Ni	0.47	0.56	0.22	98.75	<0.05	80	3.39
						136	8.5
						153	3.57 [b]
							3.42 [c]
						164	3.57

[a] Target thicknesses were homogeneous within ±10%.
[b] Target employed for isotopes with $T_{1/2} \leq 3$ h.
[c] Target employed for isotopes with $T_{1/2} > 3$ h.

TABLE II. Summary of the cross sections, recoil ranges, and backward to forward ratios for the $^{58}Ni+p$ reactions products.

Reaction product	A targ.-A prod.	σ (mb) 80 MeV	153 MeV	164 MeV	370 MeV[a]	R ($\mu g/cm^2$) 80 MeV	153 MeV	164 MeV	$B/F\times 100$ 80 MeV	153 MeV	Comments
^{57}Ni	1	79(2)[e]	56(3)	46(3)	30.5(21)	76(5)	55(3)	58(10)	7.7(6)	22(3)	
^{56}Ni	2	8.1(15)	6.0(10)	5.0(7)	3.5(2)	121(12)	84(6)	88(18)	4.3(6)	13(2)	
^{57}Co	1	78(12)	56(5)	56(6)	27(2)						b
^{56}Co	2	82(5)	63(4)	60(8)	34.6(25)	153(20)	105(6)	110(15)	4.2(11)	11(1)	b
^{55}Co	3	36(2)	23(2)	21(2)	12.0(12)	219(20)	160(10)	153(10)	2.6(7)	8.0(6)	
^{52}Fe	6	2.5(2)	2.8(3)	2.6(3)		311(25)	326(20)	290(30)	2.6(5)	5.9(3)	
^{54}Mn	4	24(3)	20(1)	18(2)		334(30)	256(10)	260(60)	4.9(15)	3.9(5)	
$^{52}Mn^g$	6	17(4)	21(2)	17(4)		350(30)	340(10)	350(50)	2.8(4)	4.4(3)	d
^{51}Cr	7	44(5)	48(2)	47(7)		370(30)	355(10)	340(40)		4.5(5)	c
^{49}Cr	9	3.3(10)		8(2)	4.9(5)						
^{48}Cr	10	0.6(1)	1.2(2)	1.2(2)	1.38(13)	440(40)	483(15)		4(2)	5.7(5)	
^{48}V	10	4.9(10)	13(1)	12(2)	16.8(18)	470(40)	455(20)	450(40)		4.6(5)	
^{46}Sc	12		0.8(1)	1.2(3)			548(55)	760(160)			
$^{44}Sc^g$	14		1.1(3)								
$^{44}Sc^m$	14		0.7(3)								

[a] Reference 20.
[b] Quoted cross sections are independent.
[c] Quoted cross sections are cumulative (parent isotopes may contribute to the quoted cross section).
[d] Parent isotope does not contribute to the ground state cross section.
[e] Numbers in parentheses represent uncertainties in the last significant digits.

TABLE III. Summary of the cross sections, recoil ranges, and backward to forward ratios for the ^{62}Ni+p reaction products.

Reaction product	A targ.-A prod.	σ (mb) 80 MeV	136 MeV	153 MeV	164 MeV	R (μg/cm^2) 80 MeV	136 MeV	153 MeV	164 MeV	$B/F\times100$ 80 MeV	153 MeV	Comments
^{61}Cu	1	12.3(4)[e]	6.8(2)	6.2(3)	5.4(2)	105(10)	69(22)	62(5)	60(8)		4(2)	
^{60}Cu	2	5.2(10)	1.9(2)	1.7(3)	1.7(2)	215(100)	120(40)	115(30)	200(50)			
^{57}Ni	5	2.3(1)	1.5(4)	1.9(2)	1.3(3)	266(20)	280(40)	198(15)	230(30)	3.5(9)	4.4(3)	
^{56}Ni	6	0.8(3)	$\leq$0.3	0.13(4)	$\leq$0.4							
^{61}Co	1	23(2)	23(4)	21(2)	26(4)	137(10)	91(5)	70(5)	70(5)		12(2)	
^{60}Co	2	32(3)	29(3)	34(2)	35(5)	205(40)		144(15)			11(3)	
^{58}Co^{m+g}	4	82(4)	61(4)	64(2)	58(2)	280(20)	250(30)	216(6)	160(20)	1.1(5)	4.4(2)	
^{57}Co	5	52(3)	46(3)	48(2)	42(4)	355(25)	300(40)	261(9)	260(25)	3.6(7)	3.5(2)	a
^{56}Co	6	6(1)	12(1)	11.4(5)	11(1)	310(40)		322(12)	325(35)		4.1(4)	a
^{55}Co	7	1.5(1)	1.4(2)	1.7(1)	1.5(2)	380(30)		348(15)	365(55)	1.3(5)	2.9(4)	
^{59}Fe	3	2.3(4)	3.1(2)	3.5(2)	3.1(3)	300(70)		179(10)	220(80)		7.7(11)	
^{52}Fe	10	0.020(5)	0.075(20)	0.13(2)	0.09(2)	390(100)	480(80)	452(30)			6(2)	
^{56}Mn	6	2.5(2)	3.3(3)	4.2(4)	3.6(3)	370(40)	360(70)	322(20)	315(50)		6.2(10)	b
^{54}Mn	8	13(1)	23(2)	28(1)	25(2)	390(40)		397(12)			4.9(3)	
^{52}Mn^{g}	10	1.5(2)	4.1(2)	4.7(3)	4.6(4)	470(40)	520(50)	475(20)			3.3(1)	
^{52}Mn^{m}	10		1.0(4)	0.5(3)	1.5(5)							
^{51}Cr	11	2.5(3)	10(1)	14.1(5)	14(1)	475(80)		490(15)			3.6(6)	b
^{49}Cr	13		0.4(1)	0.7(1)	0.6(1)		580(170)	672(60)				
^{48}Cr	14		0.02(1)	0.06(1)	0.05(1)			580(100)			4.8(15)	
^{48}V	14		1.2(3)	1.8(2)	2.1(3)			557(25)			4.4(4)	b
^{48}Sc	14			0.07(4)	0.13(3)							
^{47}Sc	15			0.3(2)								
^{46}Sc	16			0.5(1)	1.0(5)			548(65)			10(2)	
^{44}Sc^{g}	18			0.10(5)								
^{44}Sc	18			0.14(4)	0.19(3)			690(120)			8(3)	

[a] Quoted cross sections are independent.
[b] Quoted cross sections are cumulative.
[c] Numbers in parentheses represent uncertainties in the last significant digits.

in the denominator, small in comparison with the target thickness, and one obtains

$$R_F \approx \frac{1}{x} R \approx R .$$

The above approximation is generally implied in the literature where thick targets are used. Unfortunately there is no way to determine x unless one uses targets of thickness considerably smaller than projected ranges. However, one can estimate the effect of the above approximation in terms of a model calculation (see Sec. III). It was found that the projected average ranges are from 20% ($\Delta A \leq 3$) to 10% ($\Delta A > 3$) higher than the effective ranges listed in Tables II and III.

III. DISCUSSION

A. Cross sections of the radioactive reaction products

Gamma-ray activity measurements have proven to be a very effective way to determine (a) the production of nuclei which are formed with small cross section (≈1 mb), and (b) a greater fraction of the total cross section for production of various final nuclei than is possible with in-beam measurements alone. In particular, in-beam measurements miss not only direct production of a nucleus in its ground state, during the particle emission phase, but also products formed by direct feeding of the ground state via γ decay from high lying states. The importance of the contribution of the off-beam measurements to the total production cross sections is depicted in Fig. 1, from which it is obvious that in some cases as much as 50% additional cross section was found, and on the whole the observed reaction cross section was augmented by 20–30%. Without these additional cross sections a quantitative comparison of the production cross sections for various mass, A, and charge, Z, numbers with those predicted by various models, such as those performed in Ref. 2, would have not been as meaningful. Since the off-beam results were included in Ref. 2, readers are referred to that source for extensive discussion connected with the production cross sections. Only one aspect of the cross section not discussed in Ref. 2 is presented below.

In a number of radiochemical studies it has been shown (see, e.g., Ref. 13) that the spallation yield of various final nuclei following bombardment with high energy (GeV range) protons and heavier ions can be represented by

$$\ln[\sigma(A, Z)] = Y(A) + C[Z_p(A) - Z] ,$$

where $\sigma(A, Z)$ is the observed yield of a nucleus of mass A and charge Z, and the three functions Y, C, and Z_p define, respectively, the mass yield

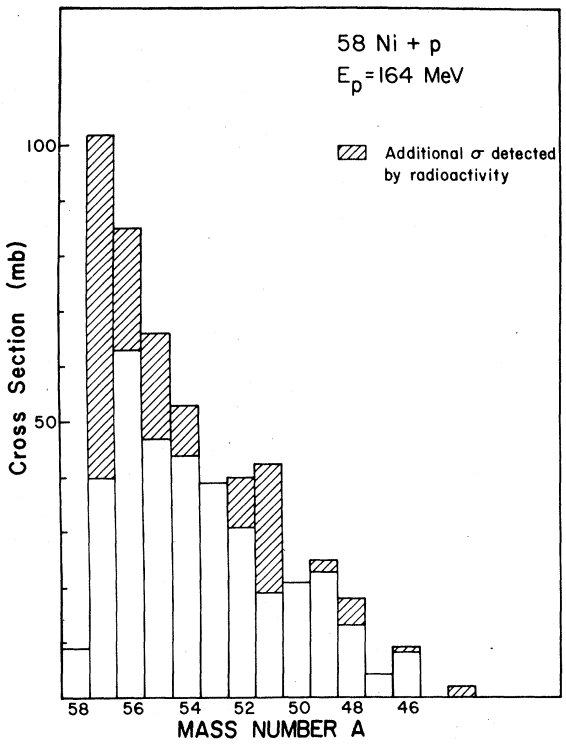

FIG. 1. Mass distribution for proton interaction with ^{58}Ni at 164 MeV incident energy. The open areas indicate the in-beam observed cross sections from Ref. 2. The dashed areas are supplementary cross sections observed through the radioactivity measurements in this work. The total observed cross section amounts to 512 mb.

curve $e^{Y(A)}$, the charge dispersion curve, and the position of the maximum yield for a given A. In such a representation the distribution of a given A-chain yield among various members of the chain is plotted against $Z_p - Z$, as is shown in Fig. 2 for the case of 164 MeV protons on ^{62}Ni target. Here both the in-beam and off-line production cross sections have been used. Nuclei whose mass A is equal to or greater than 58 were not included, since a significant fraction of their production may come from fast emission alone. The solid curve is a parabola with the parameters adjusted to best fit the data.

A comparison between ^{62}Ni data gathered at relatively low bombarding energy and natural copper data at 3.6 GeV (Ref. 13) and 28 GeV (Ref. 14) is possible due to the fact that these targets have an almost identical position with respect to the stability line; the N/Z ratio is 1.21 for ^{62}Ni and 1.19 for abundance weighted Cu, respectively. The parameters of the charge dispersion curve fitted to the experimental data of ^{62}Ni target are, within errors, identical to those[13,14] obtained for 3.9- and 28-GeV protons on natural copper. The pa-

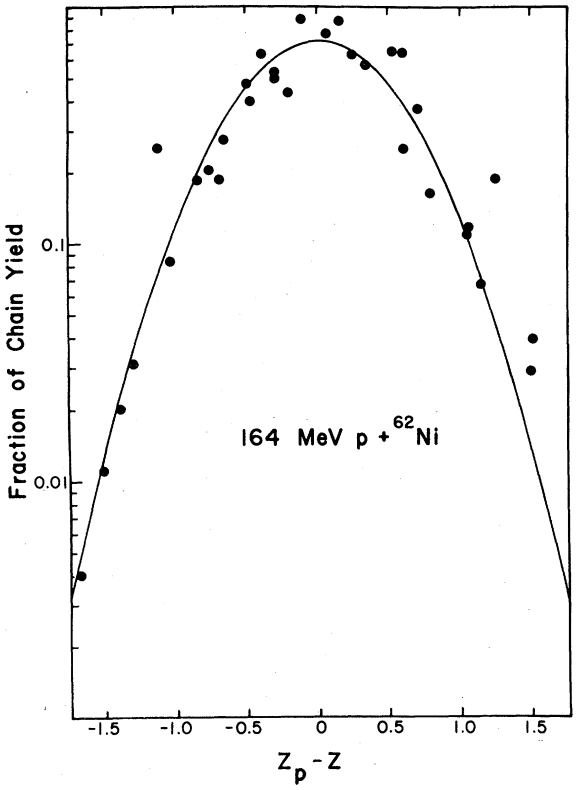

FIG. 2. Charge dispersion curve for the reaction products of 164 MeV protons interacting with ^{62}Ni. The individual cross sections are determined in this work from the radioactivity measurements and in Ref. 2 from the in-beam data. The continuous line is fitted to the data points assuming a Gaussian shape for the charge dispersion curve. The fitting procedure is described in Ref. 13. The continuous line shown in this figure fits also the 80 MeV data for ^{62}Ni target.

rameters describing the charge dispersion curve are defined and discussed in Ref. 13. The data of Fig. 2 are fitted with following values of these parameters: $X_1 = 23.41 \pm 0.05$, $X_2 = 0.455 \pm 0.008$, $X_5 = -1.77 \pm 0.04$, $X_6 = 0.73 \pm 0.04$. It is interesting to note, not only that a large variety of final nuclei fall on a common dispersion curve, but also that over a very wide bombarding energy range the characteristics of the product cross sections are remarkably similar.

B. Recoil ranges

For various final nuclei the ratios of measured forward recoil ranges R, in terms of the recoil range of the appropriate compound nucleus R_{CN}, are presented in Fig. 3. In Figs. 4–7 the observed recoil ranges vs ΔA are presented. An inspection of the trend of observed ranges leads to a number of interesting qualitative conclusions: (a) The fact that ranges of most nuclei are considerably less than R_{CN} indicates that none of these nuclei, except perhaps the lightest, were formed from the decay of projectile-plus-target compound nuclei. (b) The extremely small recoil ranges (~0.1 R_{CN}) of products near the target mass imply that these nuclei were produced in processes in which most of the incident momentum is taken away by the emitted particles. (c) Increasing values of the recoil ranges with ΔA imply that the corresponding nuclei are produced through

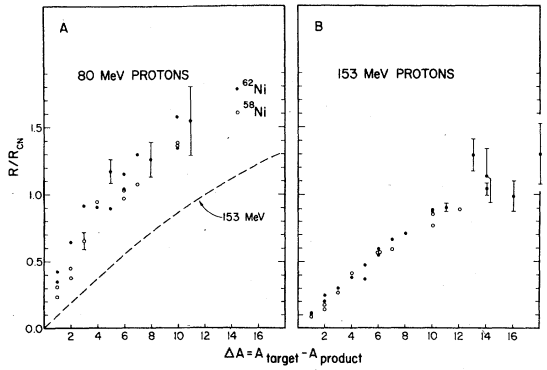

FIG. 3. The ratios of the observed forward recoil ranges R in terms of the recoil range of the compound nucleus R_{CN} for ^{58}Ni and ^{62}Ni targets. Specific final nuclei corresponding to each point in the plot can be identified using Tables II and III.

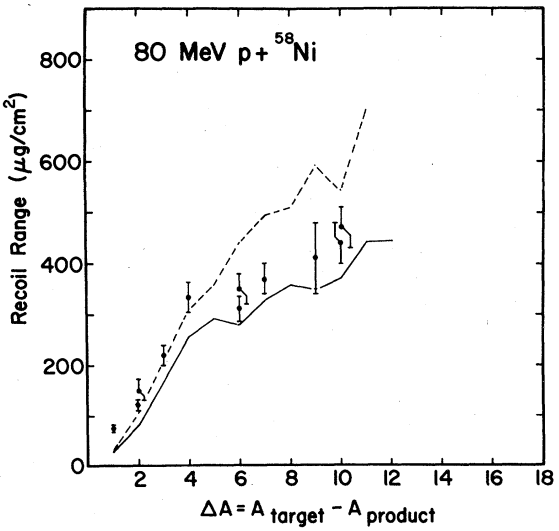

FIG. 4. The effective recoil ranges (thick target) of radioactive products determined for proton interaction with ^{58}Ni at 80 MeV bombarding energy. The indicated errors on experimental points do not include a possible 10% systematic error resulting from target thickness nonuniformity. The continuous line is drawn through the calculated values of projected recoil ranges (see text) without correction for evaporation. The dashed line includes the contribution of the evaporation momenta to the projected ranges.

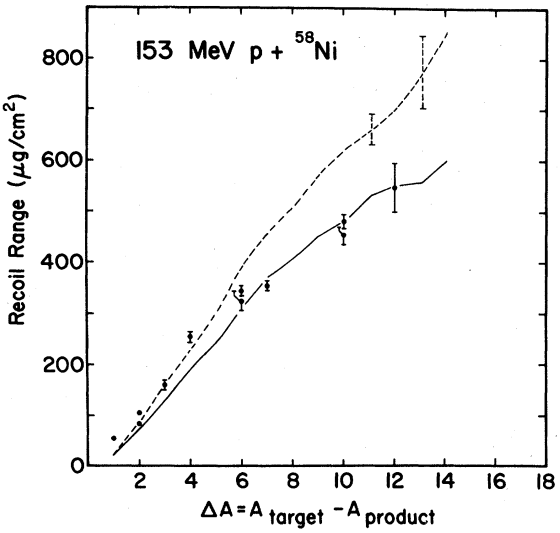

FIG. 5. The recoil ranges of radioactive products determined for proton interaction with ^{58}Ni at 153 MeV bombarding energy. (See also caption to Fig. 4.) The dashed uncertainty flags represent the statistical error caused by finite number of histories employed in the Monte Carlo calculations.

processes in which a progressively smaller fraction of the incident energy and momentum is carried out by the emitted particle.

These features are consistent with a picture of proton-induced reactions in which, as a result of interactions of the incident nucleon with the target nucleus, a few products (following the emission of some of the nucleons involved in the interactions) are left with a broad range of excitation energy.

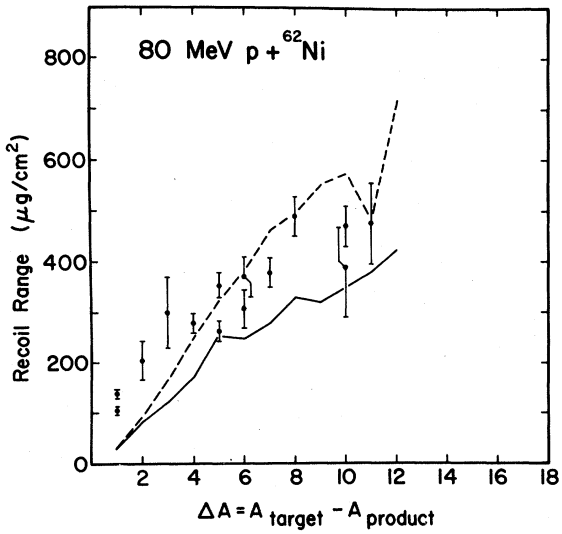

FIG. 6. The recoil ranges of radioactive products determined for proton interaction with ^{62}Ni at 80 MeV bombarding energy. (See also caption to Figs. 4 and 5.)

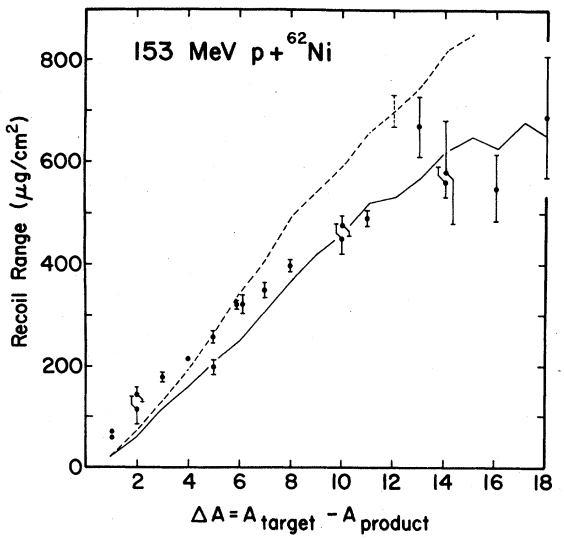

FIG. 7. The recoil ranges of radioactive products determined for proton interaction with ^{62}Ni at 153 MeV bombarding energy. (See also caption to Figs. 4 and 5.)

Most of the observed final products are produced following nucleon evaporation from these highly excited parent nuclei. Since it takes, on an average, 10 MeV of excitation energy to evaporate one nucleon, lighter final products are produced from successively higher excitations of the parent nuclei. The final nuclei, the daughters, will recoil as do their parents of appropriate excitation energy; that is, the lighter final nuclei are expected to have progressively larger recoil ranges, as is observed to be the case.

The recoil ranges of specific final nuclei were calculated in terms of the cascade model, which describes the pre-equilibrium chain of nucleon-nucleon interactions initiated by the incident nucleon, with and without incorporating the effect of evaporation on the recoil properties of the final products. The computer code used for the cascade calculations was VEGAS [3] and the evaporation computations were performed using the code DFF.[15] Both codes employ Monte Carlo techniques. Two other codes exist which are also based upon the intranuclear cascade model. One was developed by Barashenkov *et al.* at the Joint Institute of Nuclear Research [V. S. Barashenkov, K. K. Gudima, and V. D. Toneev, Acta Phys. Pol. 36, 415 (1969)]. and the second by Bertini at Oak Ridge National Laboratory [H. W. Bertini, Phys. Rev. 131, 1801 (1963); 138, 1711 (1969)]. A Comparative study of the results of the three codes [V. S. Barashenkov, H.W. Bertini, K. Chen, G. Friedlander, G. D. Harp, A. S. Iljinov, J. M. Miller, and V. D. Toneev, Nucl. Phys. A187, 531 (1972)]. indicates that they yield similar results in most

respects. A number of subroutines were added to the code **DFF** which, among other things, calculate in three dimensional space the momentum vectors of the recoiling nucleus, using the individual histories of the cascade calculation with and without the recoil momenta produced by the evaporation processes. Emission of evaporation particles (neutrons, protons, deuterons, tritons, ^{3}He, and ^{4}He) was assumed to be isotropic in the center of mass of the recoiling nucleus. For each option about 5 000 histories were sorted according to recoil energy, recoil angle, recoil range, and projected forward range of product nuclei. From the distributions so obtained, average values of the above quantities were calculated. The recoil ranges were obtained for the calculated recoil energies using the table of Northcliffe and Schilling.[10] Between zero and the lowest recoil energy for which tabulated values of recoil range are available, it was assumed that recoil ranges are proportional to recoil energy. Ranges in ^{62}Ni were obtained from those tabulated for ^{58}Ni using an appropriate mass ratio correction. The input parameters used for calculations in **VEGAS** and **DFF** codes were chosen to be the same as those which appear to give a relatively good account of

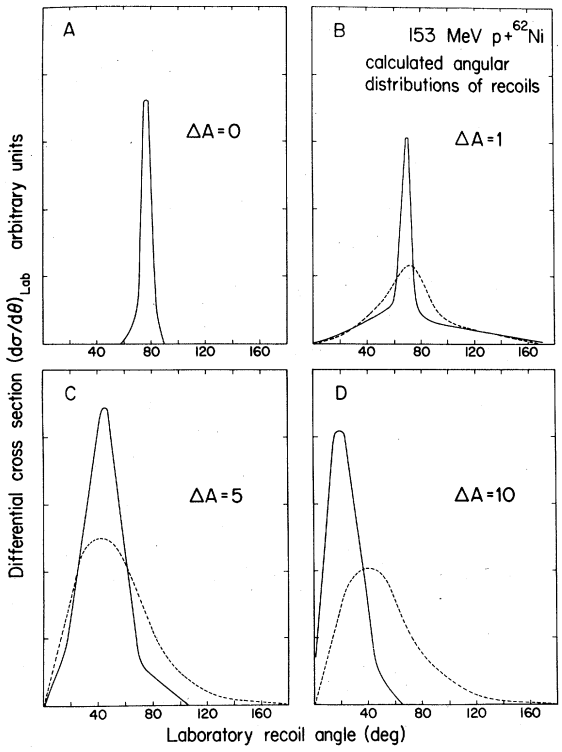

FIG. 8. Calculated (smoothed) angular distributions of recoils without (continuous lines) and with (dashed lines) the evaporation kick, for 153 MeV protons interacting with ^{62}Ni.

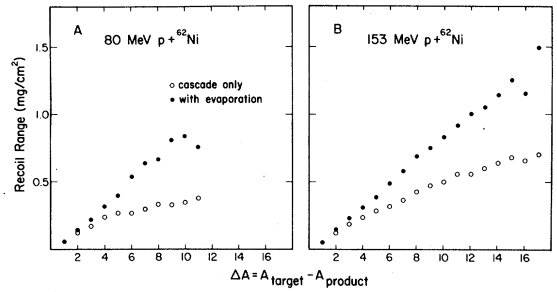

FIG. 9. Calculated nonprojected recoil ranges for 80 MeV (*A*) and 153 MeV (*B*) protons interacting with ^{62}Ni.

the inclusive production cross section as reported in Ref. 2. Some features of the results, namely angular distributions of the recoiling nuclei, nonprojected recoil ranges, and average angle of recoil with and without evaporation kick, are presented in Figs. 8–10.

The results of the calculation, for options with and without the contribution of the evaporation particle momenta, are shown in Figs. 4–7 for the cases of 80 and 153 MeV protons with ^{58}Ni and ^{62}Ni targets. An inspection of these figures clearly demonstrates that the calculations are able to give a good qualitative account of the values of the observed ranges and their trend with ΔA. Quantitatively, it appears that for the ^{58}Ni target the observed ranges are slightly higher than those calculated including the evaporation kick for nuclei within 5 nucleons from the target, but are closer to those calculated without the evaporation kick for lighter product nuclei. A similar trend is indicated for the ^{62}Ni target except that, beside relatively larger uncertainties in the measured values at 80 MeV for heavier product nuclei ($\Delta A < 4$), the measured ranges are conspicuously larger than those predicted by the calculations, even with the evaporation kick. Though the difference in this respect is larger for the ^{62}Ni target, it is in the same direction as seen for ^{58}Ni.

The backward to forward ratios are shown in Fig. 11. For heavier product nuclei the observed

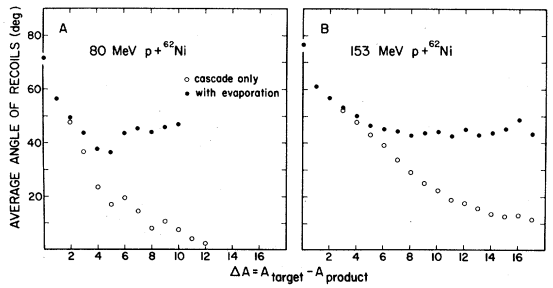

FIG. 10. Calculated average angle of recoils for 80 MeV (*A*) and 153 MeV (*B*) protons interacting with ^{62}Ni.

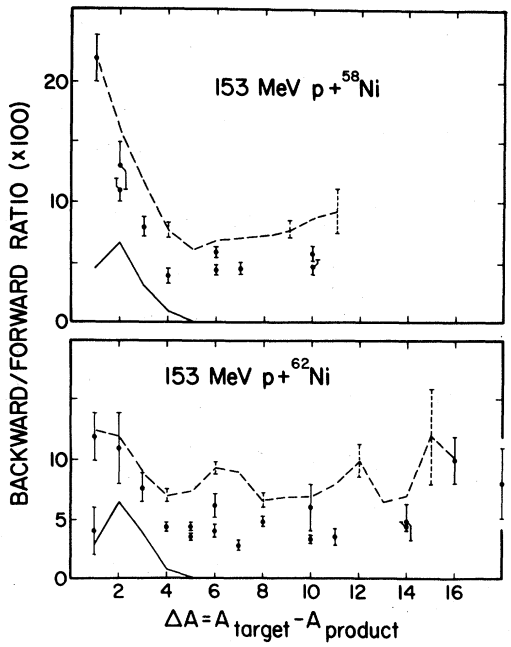

FIG. 11. The backward to forward ratio of radioactive products determined for proton interaction with ^{58}Ni and ^{62}Ni targets at 153 MeV bombarding energy. (See also caption to Figs. 4 and 5.)

B/F ratios are consistent, though somewhat lower in magnitude, with the predictions including the evaporation kick. For lighter product nuclei, however, the calculation with evaporation kick gives results consistently larger than the observed values. Without the evaporation kick only the heaviest product nuclei are predicted to show recoil in the backward direction.

The above differences notwithstanding, the key result is that the observed recoil ranges indicate an important pre-evaporation component in the interaction between the incident nucleon and the target nucleus.

The difference between the observed and the calculated ranges depicted in Figs. 4–7 can be understood to arise from a number of sources. First, the fact that the observed ranges for light products ($\Delta A \geq 6$) are consistently lower than those calculated with evaporation kick implies that this kick is overestimated in the DFF calculation. One can change values of a number of parameters in DFF to obtain a better fit to the observed ranges. Among these is the level density parameter a. The suggested[16] value of a is $A/20$ whereas $A/10$ is thought to be more reasonable.[17] The effect of the change to $A/10$ on the recoil ranges is to decrease their values by about 10%.

Some variations of other parameters, including those used in VEGAS could be made to bring the calculated values closer to the observed ones. However, the game of varying parameters to get quantitative agreement with the observed ranges was not considered justifiable unless it is accompanied by detailed comparison between the calculated and observed energies of emitted particles.

A second effect which has not been taken into account in the calculations and which can modify the recoil ranges in a significant manner is the emission of fast complex particles, such as d, t, ^{3}He, and α, in the initial fast phase of the reactions. It is known (see, e.g., Ref. 18) that about 20% of the total charged particle yield is in deuteron and α particle emission. These emissions are known to make a relatively larger contribution in the production of nuclei with large ΔA. Since the angular distribution of these particles is forward peaked, their emission would give a significant backward recoil kick which, besides reducing the average recoil momentum, would tend to increase the recoil angle. Both of these effects will tend to decrease the projected recoil ranges and enhance the number of backward recoils. Whereas this will make the comparison for forward recoils better (see Figs. 4–7) for large ΔA, it will make the comparison worse for backward recoils.

A third effect not included in the calculations and certainly affecting the measured recoil ranges is due to a change in the angle of the recoiling nucleus due to multiple atomic collision in the target prior to its escape into the catcher foil. The recoiling nucleus loses energy while passing through matter by two mechanisms, namely those involving electronic and nuclear collisions.[19] The former is the dominant process at higher recoil velocities and leads to relatively little change in the direction of the recoiling nucleus. At lower recoil velocities, as encountered here, energy loss due to both processes is contributing to the total stopping power, and since the masses of the recoiling nuclei and of the stopping atoms are comparable, at each collision significant deflection from the original direction of recoil can occur. As is obvious from Figs. 9 and 10, the average nonprojected recoil range and average recoil angle increase and decrease, respectively, as a function of ΔA for the options including and excluding the evaporation kick. For $\Delta A < 5$, evaporation does not change these values for both quantities significantly, and the lower values of observed projected range is due to the combined effect of lower recoil energy and larger recoil angle, i.e., a smaller value of $\cos\theta_{\text{recoil}}$. Nuclear collisons will tend to spread the angular distribution to a wider angular range than is indicated in Fig. 8. The effect of this spreading on the projected recoil ranges is to either increase or decrease the observed values depending upon the initial recoil direction.

In cases where the initial direction is close to 90° to the beam (as is the case for nuclei with $\Delta A < 3$, see Fig. 10) multiple scattering will throw about half of the recoils in the backward direction (thus increasing the number of backward recoils) and the other half in the forward direction. The average recoil angle of the second group will be less than the original 90° angle, effectively increasing the projected recoil ranges for the forward going segment. For nuclei with $\Delta A > 3$, the average recoil direction (see Fig. 10) is approximately 45°. The spreading around this angle due to multiple scattering tends not to change the average recoil angle, but the average (population weighted) value of $\cos\theta$ does decrease, thus decreasing the values of projected ranges for these cases.

IV. SUMMARY AND CONCLUSIONS

The cross sections for producing radioactive nuclei in the bombardment of ^{58}Ni and ^{62}Ni with 80–164 MeV protons, and their recoil ranges, have been measured. These radioactivity cross sections are found to add to the in-beam cross sections for specific nuclei to a significant degree. The properties of the charge dispersion curves are found to be remarkably similar to those observed for 3.9 and 28 GeV proton bombardment of natural copper, implying that evaporation characteristics in high and low energy bombardments are similar.

From the trend of the observed projected ranges with mass of the final nuclei, one can clearly decipher the mechanism of nucleon-nucleus reactions. It is argued that as a result of interactions of the incident nucleons with a few target nucleons, a few nuclei of mass close to that of the target are produced with a broad range of excitation. Subsequent evaporation leads to the production of most of the observed nuclei. Quantitative comparison of the observed ranges with those calculated in terms of the cascade plus evaporation models confirms that the trend and magnitude of the observed recoil ranges with ΔA are predominantly reflecting the characteristics of the preevaporation stage of the nucleon-nucleus interaction. Differences between the observed and calculated ranges may be understood as arising from (a) the choice of parameters made in the evaporation calculations; (b) neglect of the role of complex particles, such as deuteron and α emission, in the preevaporation phase of nucleon-nucleus interaction; and (c) neglect of multiple scattering of recoiling nuclei in the target material due to nuclear collisions.

ACKNOWLEDGMENTS

The authors are grateful to Dr. J. B. Cumming of the Brookhaven National Laboratory for discussions and calculations pertaining to the charge dispersion curve and to Professor G. Emery for a critical reading of the manuscript. They are also appreciative of the competent help of the IUCF technical staff in many stages of this work and in particular to Mr. B. Lozowski for the preparation of numerous targets. One of the authors (J.J.) wishes to thank IUCF management for financial support during his stay in Bloomington. This work was partly supported under an operating grant for IUCF from the National Science Foundation.

---

*Permanent and present address: Institute for Nuclear Research, Swierk, Warsaw, Poland.
†On leave from INR, Swierk, Poland.
‡Present address: LAMPF, LASL, M.S. 831, Los Alamos, New Mexico 87545.

[1]M. Sadler, J. Jastrzebski, A. Nadasen, P. P. Singh, L. L. Rutledge, Jr., T. Chen, and R. E. Segel, Phys. Rev. Lett. 38, 950 (1977).
[2]M. E. Sadler, P. P. Singh, J. Jastrzebski, L. L. Rutledge, Jr., and R. E. Segel, Phys. Rev. C 21, 2303 (1980).
[3]K. Chen, Z. Frankel, G. Friedlander, J. R. Grover, J. M. Miller, and V. Shimamoto, Phys. Rev. 166, 949 (1968).
[4]M. Blann and J. Bisplinghoff, Report No. COO-3494-27, 1975 (unpublished).
[5]A. Mignerey and M. Blann (unpublished).
[6]N. T. Porile, Phys. Rev. 120, 572 (1960).
[7]A. M. Poskanzer, J. B. Cumming, and R. Wolfgang, Phys. Rev. 129, 374 (1963).
[8]W. R. Pierson and N. Sugarman, Phys. Rev. 130, 2417 (1963).
[9]M. A. Molecke and A. A. Caretto, Jr., Phys. Rev. C 15, 719 (1977).
[10]L. C. Northcliffe and R. F. Schilling, Nucl. Data Tables A7, 233 (1970).
[11]J. Jastrzebski, H. Karwowski, M. Sadler, and P. P. Singh, Phys. Rev. C 19, 724 (1979).
[12]N. Sugarman, M. Campos, and K. Wielgoz, Phys. Rev. 101, 388 (1956).
[13]J. B. Cumming, P. E. Haustein, R. W. Stoenner, L. Mausner, and R. A. Naumann, Phys. Rev. C 10, 739 (1974).
[14]J. B. Cumming, R. W. Stoenner, and P. E. Haustein, Phys. Rev. C 14, 1554 (1976).
[15]I. Dostrovsky, Z. Fraenkel, and G. Friedlander, Phys.

Rev. 116, 683 (1959).
[16]M. Hillman, Instructions for use of the DFF program (unpublished).
[17]T. D. Thomas, Nucl. Phys. 53, 558 (1964).
[18]J. R. Wu, C. C. Chang, and H. D. Holmgren, Phys. Rev. C 19, 698 (1979).
[19]J. Lindhard, M. Scharff, and H. E. Schiott, K. Dan. Vidensk. Selsk. Mat. Fys. Medd. 33, 14 (1963).
[20]P. J. Karol and J. M. Miller, Phys. Rev. 166, 1089 (1968).